JOURNAL OF MATERIALS SCIENCE 24 (1989) 3588–3598

The optical birefringence of injection-moulded polystyrene and polyethylene

B. L. EVANS
J. J. Thomson Physical Laboratory, University of Reading, Whiteknights, Box 220, Reading, Berkshire, RG6 2AF, UK

Injection-moulded plaques of polystyrene and of two types of high-density polyethylene have been produced under different moulding conditions. Microscopic examination coupled with birefringence measurements on polystyrene and polyethylene show that the plaques contain a flow-induced molecularly ordered structure together with, in the case of polyethylene, a thin ($\sim 4\,\mu$m) disordered surface layer. Thermal annealing of the polystyrene birefringence and "frozen-in" strain distribution have been measured and interpreted in terms of phenyl group reorientation and molecular rearrangement, respectively.

1. Introduction

In an earlier publication [1], concerned with the influence of injection-moulding conditions on the properties of moulded polymer items, it was shown that, in the case of polyethylene, the surface microhardness, V_H, gave a reliable indication of the moulded polymer density, ϱ, (percentage crystallinity). As such, the measurement of V_H can give a simple, non-destructive, test of quality control in opaque or translucent moulded polymer items. In the case of transparent polystyrene however, there was no useful systematic V_H–ϱ dependence but, for this polymer, the choice of moulding conditions or degree of quality control is often assessed from the transmitted interference patterns observed when the moulding is viewed between crossed linear polarizer and analyser. Such birefringence patterns are usually interpreted in terms of the "frozen-in strain" within the moulding. This can be misleading however, because, as detailed later, the birefringence can originate from a number of causes.

This present publication is concerned with the results of an investigation in which the molecular orientation within the moulded polymer plaque is deduced from reflection, transmission birefringence measurements and microscopic examination of the crystallisable polymer polyethylene. These results are used to interpret the transmitted birefringence patterns seen in polystyrene plaques prepared under different moulding conditions and after heat treatment.

2. Experimental procedure

2.1. Plaque manufacture

Injection-moulded plaques of overall dimensions 7.5 cm × 7.5 cm × 0.3 cm were prepared from (i) high-density narrow molecular weight distribution, polyethylene homopolymer Rigidex 075-60 (BP Chemicals), (ii) high-density broad molecular weight distribution, polyethylene copolymer Rigidex 40M (BP Chemicals), (iii) homopolymer polystryene Carinex G.P. (Shell Chemicals).

The plaques were produced on a Battenfeld BSKM 90/160 in line screw preplasticizing injection-moulding machine. Molten polymer was injected through the sprue into the runners and then entered the water-cooled mould through a gate of rectangular cross-section 7.5 cm × 0.1 cm and length 0.15 cm. The axis of the gate did not coincide with that of the plaque mould but was offset as shown in Fig. 1a. The mould produced a pair of plaques as shown in Fig. 1b. One face of each plaque reproduced the highly polished mould surface whereas the opposing face carried an embossed reference grid of 1 cm squares. Points on the plaque surface will be referred to this reference grid, labelled as in Fig. 1b.

In this investigation of the influence of moulding parameters on plaque properties the front zone barrel temperature T_s and the mould temperature, T_m, were taken as the variables but there were necessary associated changes in the other moulding parameters in order to preserve surface finish and to avoid the formation of flash. A full list of the moulding parameters employed has been given earlier [1].

Each moulding is identified by three numbers, the first being the value of T_s, the second the value of T_m and the third the shot number, N, in the sequence of plaques produced after an initial run to establish the operating conditions. The polyethylene Type 40M carries the further identification letter M.

When necessary, single plaques were isolated from the complete moulding by cutting along line KK, Fig. 1, through that portion of the polymer which solidified in the gate.

2.2. Microscopic examination

Scanning electron microscope (SEM) pictures were taken of square E5 cut from plaque 180/90/1 of 075-60 polyethylene. Square E5 was first rough cut from the plaque, sub-divided into four pieces and each of the cut faces trimmed using an ultra-microtome equipped with either a freshly prepared glass knife or a diamond

0022–2461/89 $03.00 + .12

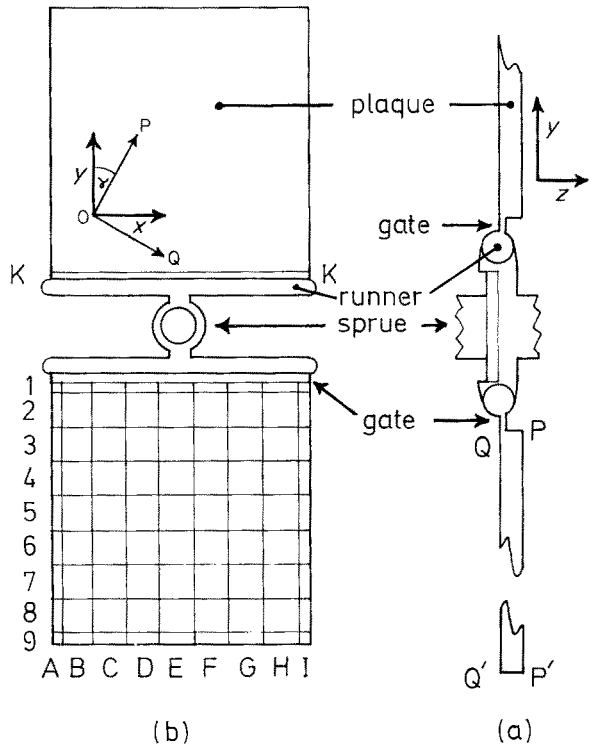

Figure 1 Side view (a) and plan view (b) of the pair of plaques obtained from the water-cooled mould. During manufacture the position of the mould is such that the plane of the plaques is horizontal.

knife. The x, y, z axes, Fig. 1, were marked on each subsection.

Prior to SEM examination, all the samples were sputter-coated with a thin film of gold.

Optical microscope measurements were made on 5 μm thick microtomed sections cut from the yz face of square E5 taken from polyethylene plaques 280/15/41M, 180/90/1 and 280/15/21. Prior to examination, each microtomed section was floated on to a gelatine-coated microscope slide which was then warmed so that the gelatine formed a sample adhesive on cooling.

2.3. Refractive index measurements

2.3.1. Polyethylene

The refractive indices of the opaque polyethylene plaques were determined by measuring the surface reflectivity using the experimental arrangement shown in Fig. 2. The polyethylene sample was mounted on a spectrometer table and illuminated with a narrow strip of collimated, linearly polarized light (wavelength 0.6 μm) chopped at a frequency of 300 Hz. Light reflected from the sample was collected by the aperture-limited spectrometer telescope whose eyepiece had been replaced by a large area photodiode. The amplified output of the photodiode passed to a phase sensitive detector (PSD) whose reference signal came from the original light chopper unit. The d.c. output from the PSD was displayed on a digital voltmeter, this reading gave a measure of the light intensity reflected from the polyethylene.

In order to determine the angle of incidence which the narrow strip of light through the collimator made with the sample surface it was necessary to determine the spectrometer table vernier scale reading corresponding to normal incidence. This was accomplished by: (1) in the absence of the sample, noting the telescope scale reading corresponding to the "straight-through" position; (2) mounting the sample and rotating the telescope to a position at 90° to the straight-through position: (3) rotating the sample to a position at which maximum light flux enters the telescope, the light was then at an angle of incidence of 45° to the sample surface: (4) rotating the sample through 45° then gave the sample (table) scale reading corresponding to normal incidence ($\theta = 0$).

Measurements of the light intensity reflected from the polyethylene surface were made by first setting the sample to give a known angle of incidence and then rotating the telescope to a position which gave the maximum output from the PSD – this output reading was then noted. In nearly every case a measurable change in the reflected light intensity (as measured by the PSD output) was observed when the angle of incidence, θ, changed by 20 minutes of arc ($\pi/540$ rad).

The light incident on the sample surface was linearly polarized, the vibration direction of the electric vector $\boldsymbol{E}$, being set either parallel (P) or normal (N) to the plane of incidence. If n_x, n_y, n_z are the principal (surface) refractive indices of the plaque for $\boldsymbol{E} \parallel x$, y, or z Fig. 1, then for light incident on the (xy) plaque surface in the (xz) plane of incidence the ratio, r_N, of

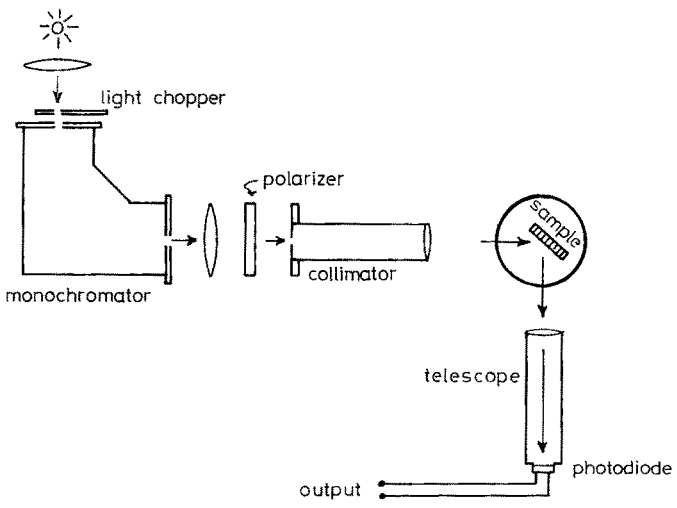

Figure 2 Experimental arrangement used to measure the light intensity reflected from a polyethylene plaque.

the reflected to incident amplitudes is given by

$$(r_N)_x^z = \frac{n_1 \cos\theta - (n_y^2 - n_1^2 \sin^2\theta)^{1/2}}{n_1 \cos\theta + (n_y^2 - n_1^2 \sin^2\theta)^{1/2}} \quad (1)$$

where the configuration is identified by stating that the z symmetry axis is normal to the boundary and the x symmetry axis lies in the plane of incidence.

Similarly,

$$\left(\frac{r_P}{r_N}\right)_x^z \simeq \left[\frac{\cos\theta - \alpha^{1/2}(1 - \gamma \sin^2\theta)^{1/2}}{\cos\theta + \alpha^{1/2}(1 - \gamma \sin^2\theta)^{1/2}}\right] \times \left[\frac{\beta^{1/2}\cos\theta + (1 - \beta \sin^2\theta)^{1/2}}{\beta^{1/2}\cos\theta - (1 - \beta \sin^2\theta)^{1/2}}\right] \quad (2)$$

where $\alpha = (n_1/n_x)^2$, $\beta = (n_1/n_y)^2$, $\gamma = (n_1/n_z)^2$ and n_1 is the refractive index of the medium through which the incident wave is travelling (in this case air, $n_1 = 1$).

Expressions for the amplitude ratios appropriate to any of the five remaining principal orientations can be determined by inspection from Equation 2. Hence

$$\left(\frac{r_P}{r_N}\right)_z^x \simeq \left[\frac{\cos\theta - \gamma^{1/2}(1 - \alpha \sin^2\theta)^{1/2}}{\cos\theta + \gamma^{1/2}(1 - \alpha \sin^2\theta)^{1/2}}\right] \times \left[\frac{\beta^{1/2}\cos\theta + (1 - \beta \sin^2\theta)^{1/2}}{\beta^{1/2}\cos\theta - (1 - \beta \sin^2\theta)^{1/2}}\right] \text{etc.} \quad (3)$$

It is evident from Equations 1 and 2 that as the angle of incidence, θ, increases from zero, so r_N increases and becomes unity when $\theta = \pi/2$. The amplitude ratio, r_P, however, first decreases and reaches a minimum (zero) value at $\theta = \theta_{min}$ where

$$\cot^2\theta_{min} \simeq \frac{n_1^2}{n_z^2}\frac{(n_z^2 - n_1^2)}{(n_x^2 - n_1^2)} \quad (4)$$

With increase in $\theta > \theta_{min}$, so r_P increases and becomes unity at $\theta = \pi/2$.

The reflected light intensities $R_P(\propto r_P^2)$ and $R_N(\propto r_N^2)$ were measured as a function of θ for the moulded (xy) surfaces of the polyethylene plaques and the microtomed (yz) surfaces from which the sections analysed in Section 2.2 were obtained. Measurements of $[R(\theta)]_x^z$, $[R(\theta)]_y^z$ were made on the moulded surfaces of samples 280/15/31, 280/55/11, 280/90/31; 180/90/11M and 180/15/31M. In the case of the microtomed surfaces the sample dimensions were such that only $[R(\theta)]_z^x$ could be measured for samples 280/15/21, 180/90/1 and 280/15/41M.

2.3.2. Polystyrene

The "white-light" refractive index of each glass-clear polystyrene plaque was found by measuring the real and apparent thickness of the plaque at the centre of a grid square E5.

Every polystyrene plaque exhibited a birefringence pattern when viewed in white light through crossed linear polarizer and analyser. The sign of the birefringence and the relative retardation giving rise to the transmitted colour at a particular point in the plaque was determined using a quartz wedge. All birefringence patterns were recorded with the $\boldsymbol{E}$ vector of the polarized wave parallel to the y plaque axis.

2.4. Heat treatment

The polystyrene plaques were heat treated in a thermostatically controlled ($\pm 1°$ C) circulating silicone oil bath. Polystyrene does not absorb or dissolve in silicone oil even at 99° C [2].

3. Experimental results

3.1. Visual appearance of plaques

The design of the mould was such that plaques of different thickness could be produced by altering the position of plate PP′ with respect to plate QQ′, Fig. 1a. Polyethylene plaques 0.1 cm thick showed two-dimensional curvature due to residual strain, the centre of curvature being below PP′. The 0.3 cm thick polyethylene and polystyrene plaques used in this investigation were not visibly distorted.

Visually the 075-60 and Type 40M polyethylene plaques appeared identical. Both types were opalescent and on nearly all the plaque surfaces flow marks were evident in the vicinity of the moulding gate. Away from the gate area the plaques retained the highly polished surface of the mould, one face of each plaque also carried the reference grid described in Fig. 1. The "glass-clear" polystyrene plaques did not show flow marks.

3.2. Plaque surface roughness

The smoothness, or otherwise, of the plaque surface is primarily determined by that of the mould surface with which it was in contact. Talystep traces were made of the polyethylene and polystyrene xy plaque surfaces in the y and x directions. In the y direction, Fig. 1, both plaques exhibited fine-scale surface roughness of amplitude $\leqslant 0.02\,\mu$m. In the x direction, however, there was large amplitude ($\leqslant 0.5\,\mu$m) surface roughness, evidently associated with the mould machining operations, in addition to the fine-scale roughness.

3.3. Microscopic examination of polyethylene plaques

SEM measurements were made on square E5 cut from plaque 180/90/1 of 075-60 polyethylene, the most dense polyethylene sample available [1]. Each face of the sample was trimmed by ultramicrotome and it was found that even when great care was taken the surface was invariably damaged by the cutting action. In the worst cases this damage consists of "scoring" of the surface by debris collected on the microtome knife, while in the comparatively "score free" region at the beginning of the cut the surface is smeared by plastic flow. This is illustrated in Fig. 3 which shows a portion of the xz surface produced near the beginning of the microtome stroke, the cutting direction is evident from the plastic flow pattern which produced an undulating surface. Fig. 4 shows a higher magnification view of this area in which a fibrous structure is evident (cross-sectional diameter $\sim 0.1\,\mu$m), which may be associated with the bulk material.

Optical microscopic measurements were made on 5 μm thick sections cut, by microtome, in the y direction from the yz face of square E5 of plaques 280/15/41M, 180/90/1 and 280/15/21 which lie near the

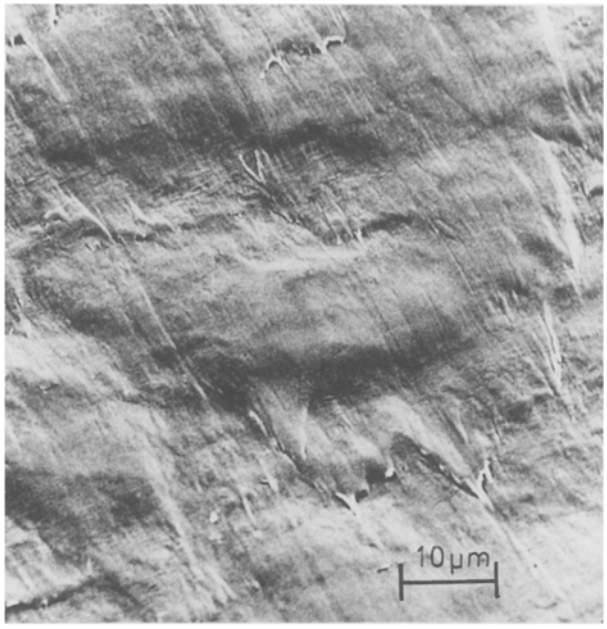

Figure 3 Scanning electron micrograph of a portion of the *xz* surface of a section cut from plaque 180/90/1 of 075-60 polyethylene. The cutting direction of the ultramicrotome is evident from the plastic flow pattern.

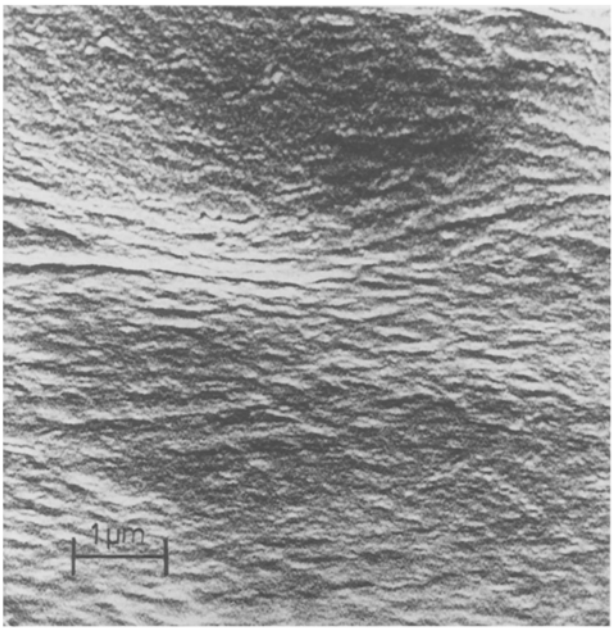

Figure 4 A higher magnification SEM picture of the area shown in Fig. 3. The fibrous nature of the surface is now evident.

extremes of the V_H–ϱ characteristic [1]. It is evident from Fig. 3 that such thin microtomed samples must inevitably have been damaged and the transmitted light optical measurements must be treated with caution.

When viewed between crossed polarizer and analyser all the microtomed sections were found to be birefringent with principal axes in the *y* and *z* directions.

Fig. 5 shows part of the 280/15/21 sample section including the long edge which contains the *xy* surface. This optical transmission photograph clearly shows the fibrous nature of the polymer section. When focusing at different levels through the section it is seen that the situation shown in Fig. 5 pertains throughout 5 μm thickness of the section. It is difficult to estimate the fibre length from Fig. 5 because individual fibres move in and out of the focal plane. However, it is evident that many of the fibres are at least 30 μm in length. Pictures similar to Fig. 5 are obtained at all positions across the sample slice showing that the fibre orientation (perpendicular to the *xy* surfaces of the plaque) is maintained throughout the entire thickness of the plaque apart from an approximately 4 μm thick layer at the *xy* plaque surfaces where the fibre orientation changes. Away from the *xy* plaque surfaces there was no evidence of stratification of the type previously reported [3–5].

Transmission optical microscope pictures of 5 μm thick slices taken from plaques 280/15/41M and 180/90/1 were essentially similar to Fig. 5. There was no quantifiable difference that could be attributed to the different densities of these plaques [1].

3.4. The refractive indices of moulded plaques

3.4.1. Polyethylene

The reflectivity measurements from the moulded plaque surfaces are typified by the graphs given in Fig. 6 which show $(R_P)_x^z$ and $(R_N)_x^z$ for sample 180/90/11M. Note that, in accordance with Equations 1 and 2 R_N increases continuously with increase in θ whereas R_P shows a minimum at $\theta = \theta'_{min} = 56° 22'$. Hence Equation 4 becomes

$$\cot^2\theta' = 0.4425 = \frac{1}{n_z^2}\frac{(n_z^2 - 1)}{(n_x^2 - 1)} \qquad (5)$$

In the orthogonal orientation, plaque 180/90/11M showed a minimum in $(R_P)_y^z$ at $\theta'_{min} = 56° 31'$. Because

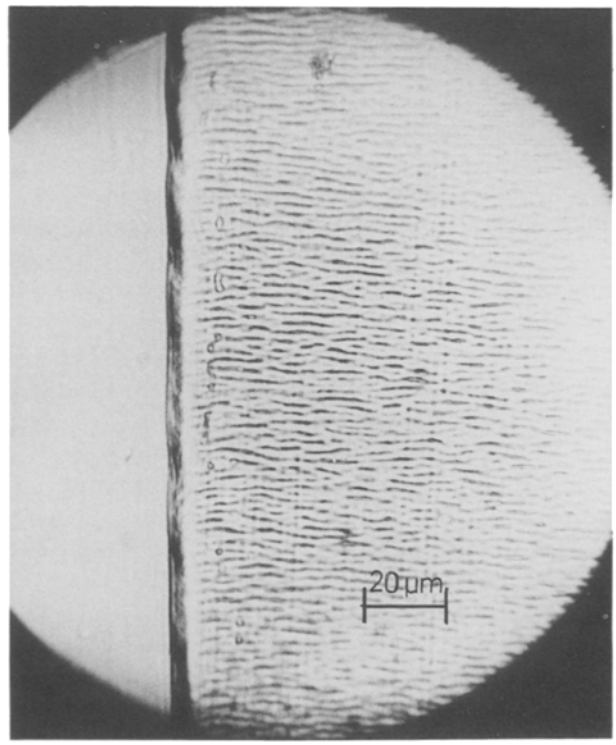

Figure 5 A transmission optical micrograph of a 5 μm thick section cut from the *yz* face of square E5 of polyethylene plaque 280/15/21. The fibre orientation is perpendicular to the edge of the sample (the *xy* plaque surface).

the measurements are limited to an angular sensitivity of 20 arc minutes the similarity in these θ' values indicates that, at the xy plaque surface, $n_x = n_y$. Similarly, within experimental uncertainty, it was found that $n_x = n_y$ for samples 180/15/31M, 280/90/31, 280/55/11 and 280/15/31.

In order to measure n_x and n_z, reflectively measurements were made on the microtomed yz faces of square E5 prepared from polyethylene plaques 280/15/21, 180/90/1 and 280/15/41M. The only experimental arrangement possible measured $(R)_z^x$ in which case a minimum in $(R_P)_z^x$ was observed at angle $\theta = \theta''_{min}$ where, cf. Equation 4

$$\cot^2\theta'' = \frac{1}{n_x^2}\frac{(n_x^2 - 1)}{(n_z^2 - 1)} \quad (6)$$

Equations 5 and 6 combine to give

$$n_x = \frac{\sin\theta''}{\cos\theta'}, \quad n_z = \frac{\sin\theta'}{\cos\theta''} \quad (7)$$

Substituting the measured values of θ' and θ'' in Equation 7 gave

Sample 280/15/21: $n_x = 1.505$, $n_z = 1.493$

Sample 180/90/1: $n_x = 1.509$, $n_z = 1.471$

Sample 280/15/41M: $n_x = 1.511$, $n_z = 1.495$

The reflectivity measurements show that in all three samples, the yz face is birefringent. This is in agreement with the optical transmission measurements on the 5 μm thick slice, 3.3. The sign of the birefringence is such that the refractive index, n_x, for $E\perp$ fibrils is greater than the refractive index n_z for $E\parallel$ fibrils.

3.4.2. Polystyrene

There was no measurable variation in the "white light" refractive indices of polystyrene plaques moulded under different conditions, the mean value obtained was $n = 1.534 \pm 0.045$ compared with the manufacturers quoted value of $n = 1.59$.

If the moulded polystyrene plaque contains orthogonal birefringent axes OP, OQ which are parallel to the surface and, at a given point, are inclined at angle α to the y axis, Fig. 1, then when viewed between crossed polarizer ($E \parallel y$) and analyser the transmitted wave is given by

$$E_t = E_0 \sin 2\alpha \sin\frac{\phi}{2} \exp i\left(kz - \omega t - \frac{\phi}{2} + \frac{\pi}{2}\right) \quad (8a)$$

where ϕ is the relative phase retardation introduced by passage through the plate thickness, d, i.e.

$$\phi = 2\pi r/\lambda \quad (8b)$$

and r is the relative path retardation.

If the birefringent axes are a consequence of applying a uniaxial stress P to a previously isotropic plate then, within the elastic region,

$$r = CPd \quad (8c)$$

where C is the stress-optic coefficient.

The transmitted light intensity (proportional to E_t^2) will be zero if either $2\alpha = n\pi$ or $\phi = 2n\pi$, the latter condition being equivalent, Equation 8b, to $r = n\lambda$ where $n = 0, 1, 2$, etc.

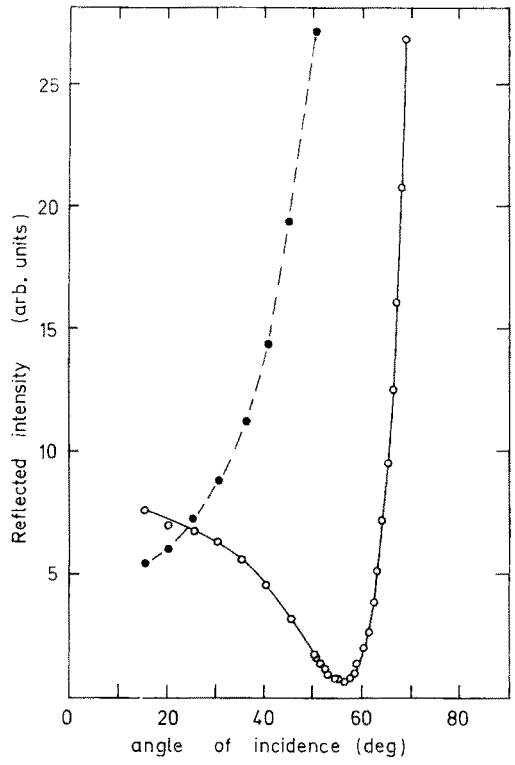

Figure 6 The measured reflectivity (○) $(R_P)_x^x$ and (●) $(R_N)_x^x$ of polyethylene plaque 180/90/11M as a function of the angle of incidence.

The condition $2\alpha = n\pi$ means that the principal axes OP, OQ are parallel to the polarizer and analyser directions. At every point in the plate where this occurs the intensity is zero whatever the wavelength or magnitude of r. The locus of such points gives the black isoclinic fringes.

The second condition of zero transmitted intensity, $r = n\lambda$, depends upon the light wavelength, λ. If white light is used, then at all points of equal retardation, r, the same colour will be transmitted. Thus, moving in the direction r increasing the transmitted colour changes from black through red and blue to green corresponding to successive extinctions of blue, green and red.

Fig. 7a shows the birefringence pattern in as-prepared plaque 250/65/22. The black isoclinic running in the y direction down the centre of the plaque and broadening to the full width of the plaque at the end remote from the gate, indicates the area in which either the principal refractive indices are parallel to x, y or the plaque is isotropic. The coloured "hoop" fringes are the isochromats of equal relative retardation where the birefringent axes are no longer parallel to x, y. Superimposing the quartz wedge, as shown in Fig. 7a, produces a black "fringe" at a position where the sum of the relative retardations is now zero, i.e. the plaque refractive index in the wedge direction is less than that in the orthogonal direction.

For comparison, Figs 7b and c show the birefringence patterns observed in the as-prepared plaques, 210/40/22 and 170/15/22, i.e. in the sequence of diminishing T_s, T_m.

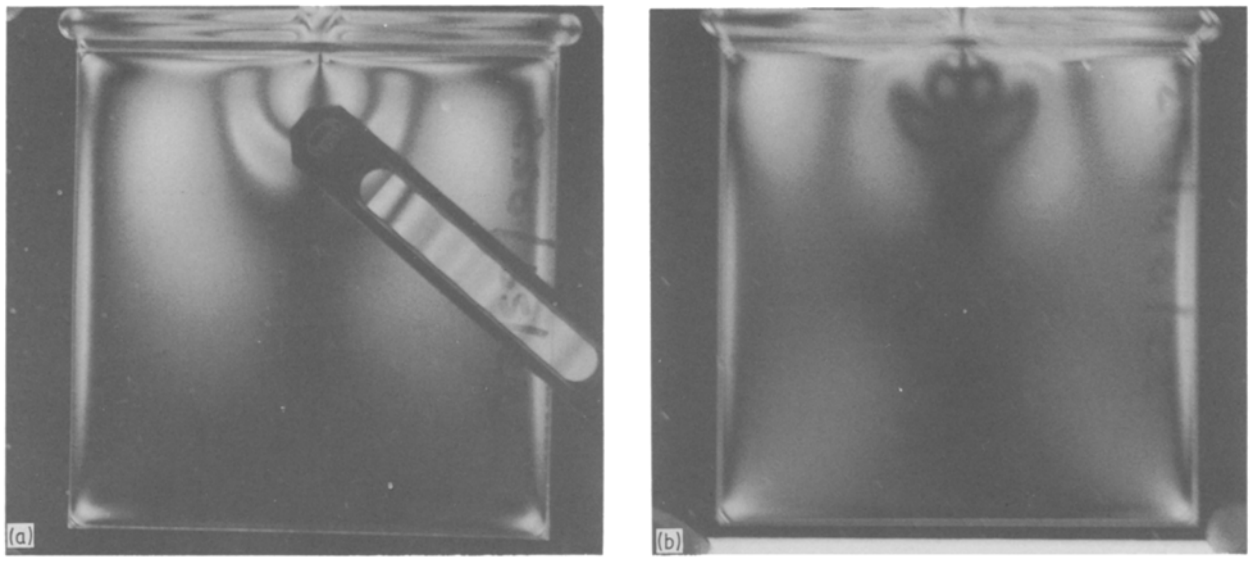

Figure 7 Monochrome reproduction of the coloured birefringence patterns observed in "as-prepared" plaques of polystyrene: (a) 250/65/22, (b) 210/40/22, (c) 170/15/22. All patterns were obtained with the ***E*** field of the incident wave parallel to the plaque y direction, Fig. 1. Superimposing a quartz wedge, (a), produces a black fringe at a position where the sum of the relative retardations is zero.

3.5. Heat-treated polystyrene plaques

When the polystyrene plaques were thermally annealed in the silicon oil bath at 100° C for 1 h, the birefringence patterns virtually disappeared and the plaques assumed the distorted shapes shown in Figs 8a to c, the plaque distortion increasing in the sequence 250/65/22, 210/40/32, 170/15/32. The centre of curvature of each plaque is below that face of the plaque in line with the moulding gate. This direction of curvature was also evident in 0.1 cm thick plaques which had not been heat treated and suggests that the "frozen-in" stress distribution is unbalanced due to the non centro-symmetric gate, Fig. 1b.

A quantitative measure of the plaque distortion produced by the heat treatment was obtained using a spherometer. The height, h (cm), of the spherometer centre leg above the plane of the three fixed legs was measured at the centre of reference square E5, Fig. 1. The radius of curvature $R \simeq 8/3h$.

Because heat treatment at 100° C is obviously too drastic, a new set of plaques was heated for 1 h at 78° C. There was then no evidence of distortion or change in the birefringence patterns which agrees with an earlier observation [6]. It was eventually discovered that a slow but measurable annealing rate was obtained by heat treatment in oil at 88° C. The heat treatment at 88° C was interrupted at regular intervals in order that the birefringence pattern and the value of h for each plaque could be recorded. Fig. 9 shows the measured variation in h with heating time, t, up to 1013 h and Figs 8d, e, f show the birefringence patterns obtained at 7.5 h. There was very little change in the birefringence patterns for $t > 7.5$ h.

At the end of the 88° C heat treatment the plaques were further heated at 100° C for 25 h to find the final values of h. These were: plaque 250/65/22 (h_f = 0.373 cm), 210/40/22 (h_f = 0.565 cm), 170/15/22 (h_f = 0.565 cm), i.e. the last two plaques achieved the same final distortion but at different recovery rates, Fig. 9.

The "as-prepared" polystyrene plaque ($h = 0$) evidently contained a frozen-in stress distribution $S = S_0$. In the thermally annealed plaque ($h = h_f$), $S = 0$. Assuming a linear relationship between S and h then

$$S = S_0 (1 - h/h_f) \quad (9)$$

If, at a given annealing temperature, S decays as

$$S = S_0 \exp(-\alpha t) \quad (10)$$

where t is the annealing time then

$$\ln (1 - h/h_f) = -\alpha t \quad (11)$$

where α is a decay constant appropriate to the particular annealing temperature and stress-relief mechanism. Fig. 10 shows the measurements of Fig. 9 plotted in the form of Equation 11. All three plaques show a final annealing stage in which $\alpha = 1.2 \times 10^{-4}\ h^{-1}$, in the case of plaque 250/65/22 this value of α applies throughout the entire annealing process. Plaque 170/15/22 shows two earlier stages, an initial stage in which $\alpha = 4.6 \times 10^{-2}\ h^{-1}$ and a second stage having $\alpha = 2.6 \times 10^{-2}\ h^{-1}$, while plaque 210/40/22

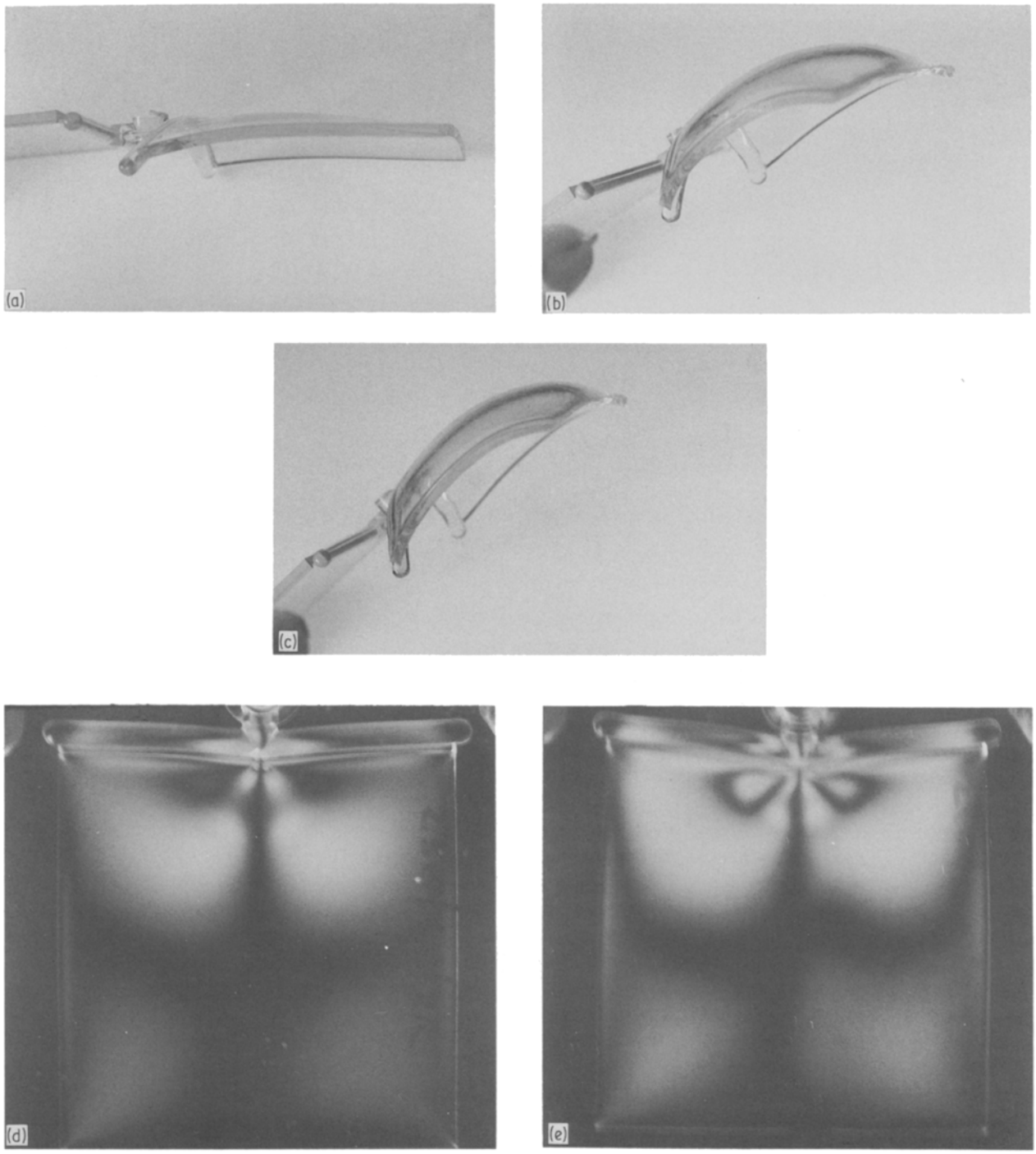

Figure 8 The effect of heat treatment on the injection-moulded polystyrene plaques. Heat treatment at 100° C for 1 h distorted the plaques as shown in (a) 250/65/22, (b) 210/40/32 and (c) 170/15/32. Heat treatment at 88° C for 7.5 h reduced the "as-prepared" birefringence patterns, Figs 7a, b, c, to those shown in (d) 250/65/22, (e) 210/40/22 and (f) 170/15/22.

has one earlier stage (the initial stage) in which $\alpha \simeq 10^{-2}\ h^{-1}$. It is difficult to define Stage 1 on the 210/40/22 graph in Fig. 10 and it is possible that the value of α, and hence the recovery mechanism, may be the same as that of Stage 2 in plaque 170/15/22. On that interpretation it would appear that the moulding process can introduce three types of strain defect in the polystyrene plaques, the occurrence of these defects being related to the moulding conditions.

In principle the thermal activation energy of each

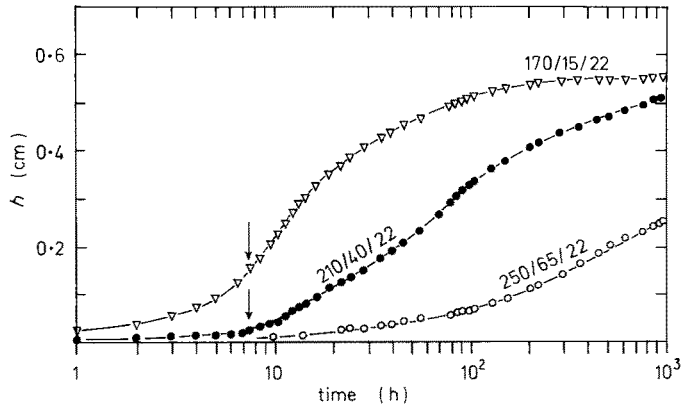

Figure 9 The distortion, h, produced in plaques (○) 250/65/22, (●) 210/40/22 and (▽) 170/15/22 as a function of annealing time at temperature 88°C. The arrows denote the annealing time $t = 7.5$ h at which the birefringence patterns shown in Figs 8d, e, f were obtained.

annealing process shown in Fig. 10 could be determined by measuring α as a function of temperature. However, the limited temperature range over which such measurements can be made would severely limit the accuracy of the results.

4. Discussion

4.1. Polystyrene

4.1.1. Optical properties of polystyrene

The optical properties of polystyrene are interpreted in terms of a model in which some degree of polarizability anisotropy is associated with the hydrocarbon "backbone" chain but the major part of the anisotropy is associated with the phenyl side groups. This is illustrated in Fig. 11 where the arrows, indicating the approximate magnitudes and directions of the principal polarizabilities, show that the polarizability of the phenyl ring is approximately twice as great in the plane of the ring as in a direction perpendicular to that plane. The ring is a rigid planar structure which has no internal degrees of freedom, the only motion possible is a rotation around the bond connecting it to the chain backbone. In the isolated molecule, phenyl groups attached in the *trans* sequence will be orientated such that the normal to the plane of the phenyl group is parallel to the local axis of the chain backbone. In the solid the phenyl group orientation may be disturbed by molecular–molecular interactions thereby reducing the correlation between phenyl group and molecular backbone orientation.

In the case of unorientated polystyrene in the glassy state, the application of a tensile stress is thought [7] to rotate the phenyl groups so that they tend to align in the stress direction giving the observed [8–14] positive stress-optical coefficient $C \simeq +10$ Brewsters at room temperature [7]. The numerical value of C increases from +9 Brewsters in high molecular weight polystyrene (mol wt > 80 000) to +11.6 Brewsters in low molecular weight samples (mol wt ≃ 50 000) [15]. This effect can probably be explained on the basis that the monomer units, and hence phenyl groups, near the end of the chain have more flexibility and freedom to orientate than those within the chain. These end groups will make C more positive to an extent depending on the concentration of chain ends in the polymer, which is determined by the number average molecular weight.

A calculation in which the glassy polystyrene was represented by a system of discs (phenyl groups) randomly distributed throughout an elastic medium gave a positive stress-optical coefficient approximately twice the observed value [7].

For stresses applied in the rubbery state above the glass transition temperature the semi-mobile polymer chains are able to align in the stress direction and consequently the plane of the phenyl groups tends to be at right angles to this direction giving the observed [13, 14, 16, 17] negative stress-optical coefficient C which varies with time.

Some degree of molecular orientation can be introduced into a glassy polymer by a procedure in which a uniaxial stress is applied to the sample which is then

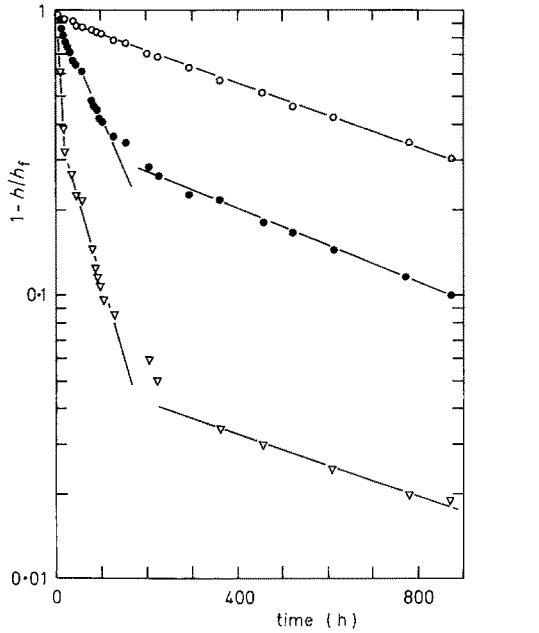

Figure 10 The measurements of Fig. 9 plotted in the form of Equation 11.

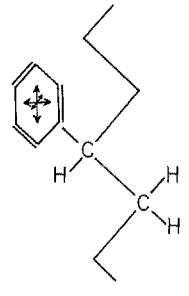

Figure 11 Schematic diagram of the Styrene molecule. The arrows indicate the approximate magnitudes and directions of the principal polarizabilities of the phenyl group.

raised to a temperature slightly above the glass transition temperature. The sample is held at this temperature and allowed to creep to a suitable extent to give the orientation required and then, while still under load, quickly cooled to room temperature. The load is removed. As a result of the molecular orientation introduced the samples become negatively birefringent [8–10, 18], the magnitude of the birefringence $\Delta n = |n_{\parallel} - n_{\perp}|$ increasing with the degree of ordering. In order to account for this negative birefringence it is necessary [19] for the plane of the phenyl ring to lie not in the plane containing the orientated chain backbone (which would produce approximately zero birefringence) but in a plane roughly perpendicular to it. Over the temperature range -196 to 50° C the magnitude of the orientation birefringence is almost independent of temperature which suggests that rotational motion of the phenyl ring is sterically hindered [20].

If some degree of molecular orientation is present in a glassy polystyrene sample then the stress-optic coefficent, C, while still positive, is different to that of the unordered material. When the stress is applied in the orientation direction, C decreases from the value $+10$ Brewsters, characteristic of the unorientated sample ($\Delta n = 0$), to $+4$ Brewsters in the most highly orientated material ($\Delta n = -0.04$) [21].

In the case of liquid polystyrene, molecular orientation can be produced if the liquid is forced to flow along an enclosed channel. The molecular orientation is a consequence of the viscous shear forces associated with the velocity profile, i.e. a static boundary layer and a velocity maximum in the centre of the channel. The orientational birefringence associated with such steady isothermal flow varies linearly with the shear stress and is independent of temperature [22].

4.1.2. Birefringence in injection-moulded polystyrene

The birefringent patterns observed in the injection-moulded polystyrene plaques, Fig. 7, may originate from a number of causes.

4.1.2.1. Flow induced birefringence. It has been suggested that the birefringence due to molecular orientation in the moulded glassy state is merely the "frozen-in" flow-induced birefringence of the melt [22, 23]. Support for this idea came from experiments in which (a) the birefringence-shear stress relationship for molten polystyrene gave a reasonable description of the variation in measured peak birefringence with estimated injection shear stress in moulded plaques [22]; (b) a thin film of molten polystyrene was sheared between parallel glass plates. The solidified film exhibited the negative orientation birefringence associated with the molten state. Plotting the measured glass birefringence against the stress, in the molten state, which produced it gave a stress-optical coefficient, C, for the vitrified samples of 4500 Brewsters [23] which is close to that for the molten polymer.

In Section 3.4.2, Fig. 7, it was shown that the polystyrene plaques were negatively birefringent along the normal to the isochromatic fringes usually associated with the flow pattern. If the phenyl group orientation also defines the molecular chain orientation (Section 4.1.1), then the birefringence patterns of Fig. 7 do indicate the molecular orientations which prevailed when the liquid filled the mould. On this interpretation the form of the liquid flow front during the filling stage will be similar to that shown in Fig. 12.

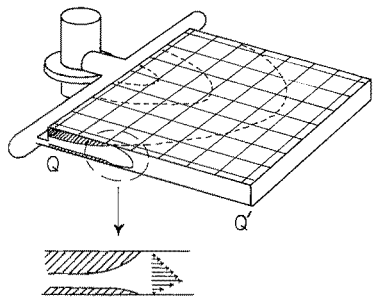

Figure 12 Anticipated form of the melt front filling the mould.

Mould filling by a developing front has been the subject of detailed mathematical analysis based on hydrodynamic lubrication theory [24–33].

Viewed perpendicular to the narrow cross-section of the mould there is a solidified layer growing out from the walls, Fig. 12, and an approximately isothermal hot core through which the melt flows in a Posseuille-type shearing motion. At the front the melt from the centre region flows outwards like a fountain to the mould walls where it solidifies. After the mould is filled the melt becomes stationary and cools and vitrifies under the action of the applied pressue. Calculations of the pressure distribution throughout the mould during the filling process requires a realistic model of the melt and has to take into account the dependence of polystyrene viscosity on pressure [34] and temperature [35].

As far as molecular orientation within the vitrified layer is concerned, it is thought that near the mould wall the orientation is that associated with the fountain flow at the flow front, Fig. 12. Moving away from the wall, the orientation will be associated with the stream line flow of the melt as it passes between the vitrified walls. The thickness of the vitrified layers at the end of the filling stage will depend upon the mould wall temperature, injection rate, etc. At the centre of the moulding where the melt vitrified under quasi-static conditions there may be no nett molecular orientation.

The distribution of birefringence in injection mouldings has invariably been measured by cutting thin slice from the moulding and assuming that this did not change the birefringence. In the case of injection-moulded polystyrene strips the gapwise (negative) birefringence distribution, the measurements apparently being in the xy plane, showed zero values at the centre and surface with a maximum in between [36]. Other investigators have confirmed the existence of the birefringence maximum (at a position approximately three-quarters of the distance from the centre to the mould walls [22, 32, 35, 37, 38]) but found a birefringence minimum between this maximum and the surface with large birefringence values at the surface and small, but non-zero, values at the centre [32, 35, 37, 38].

In general it has been found that the magnitude of

the maximum birefringence increases with decreasing wall mould temperature, T_m, and the birefringence patterns of Fig. 7 support this conclusion. Theoretically, however, it is predicted [33] that the primary parameters affecting residual stresses and orientation (as assumed associated with birefringence) are the flow rate and melt temperature, T_s; both of these factors should be maintained at the highest permissible levels thereby accelerating the relaxation of stresses which arise during mould filling.

The observations that the magnitude of the plaque birefringence increases with decreasing T_m, T_s and that the birefringence is detectable at greater distances from the injection gate, Fig. 7, can be attributed to one or more of the following related effects. (a) There is an associated increase in the degree of flow-induced molecular orientation due to the necessary change in operating parameters [1]. (b) At any one position in the plaque there is an increased thickness of orientated vitrified layer. (c) The lower temperatures reduce thermal annealing of the birefringence at the end of the filling stage. This latter effect could also be important in connection with any stress-induced birefringence.

4.1.2.2. Stress-induced birefringence. Another characteristic of injection mouldings that can play an important role in determining the birefringence and mechanical properties is the residual stress state resulting from thermal gradients set up during solidification in the mould. The interior of injection mouldings is normally in a stage of tension while the material near to the surface is in compression [39–42]. This "frozen-in" stress distribution will contribute to the birefringence through the photoelastic stress effect, Equation 8c, the magnitude of this contribution again depending upon any molecular orientation that is present.

In the injection-moulded polystyrene (and polyethylene) plaques the frozen-in stress (strain) distribution is non-symmetric due to the offset gate, Fig. 1. This results in the thermally annealed plaques assuming the shapes shown in Figs 8a, b, c. If the maximum velocity of the liquid flow front during mould filling is along the centre line of the gate, Fig. 12, then the centre of curvature of the annealed plaque is on that side of the centre line having the greatest velocity gradient and hence shear stress (and molecular orientation). The birefringence patterns achieved their final state, Figs 8d, e, f at a very early stage in the annealing process, Fig. 9, before any appreciable molecular disorganization had taken place. This was evidently the result of the phenyl group reorientation, the molecular disorganization (accompanying stress relaxation and producing distortion) occuring at a much slower rate and apparently by a three-stage process, Fig. 10.

4.2. Polyethylene

4.2.1. Structure and optical properties of polyethylene plaques

An important distinction between polyethylene and polystyrene arises because polyethylene is a crystallizable polymer (exhibiting mass fraction crystallinities in the range 20 to 80%) whereas atactic polystyrene is

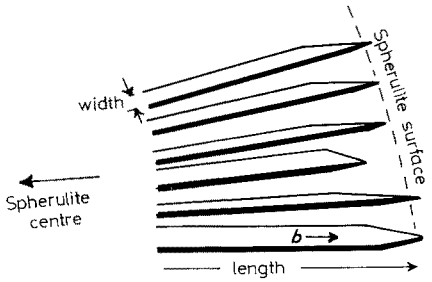

Figure 13 Simplified model of part of a spherulite in polyethylene which consists of a radial array of chain folded crystalline lamellae having their crystallographic *b*-axis (of the orthorhombic structure) in the radial direction, i.e. the molecular orientation is perpendicular to a radius. The lamellae, which are typically 20 nm thick, 5 μm wide and up to 30 μm long in a spherulite of 100 μm diameter, can have a variety of forms, i.e. {2 0 1} ridged sheets in various orientations about the radial *b* direction, or planar (or slightly curved) {2 0 1} sheets or S-shaped sheets [43].

not. In the absence of any applied stress a crystallizable polymer solidifies in the form of a spherulitic aggregate. The detailed structure of one such spherulite is shown in Fig. 13. It is composed of a radiating array of ribbon-like crystals, which are very long in comparison to their thickness, the thickness of each ribbon being of the order 10 nm. The polymer chains are arranged approximately parallel to the thin dimension of the ribbon; each chain may enter a given crystal ribbon many times. The crystal ribbons are connected by "tie chains", i.e. chains incorporated into adjacent crystallites of an array but the inter-ribbon region is predominantly non-crystalline and therefore less dense than the crystalline region. Because of the density (and hence refractive index) discontinuities at the crystalline–non-crystalline interfaces, light scattering can occur giving rise to the opalescent appearance of the solid.

Polyethylene and polystyrene both possess the same hydrocarbon backbone chain, Fig. 11, but in polyethylene the phenyl side groups are replaced by hydrogen atoms. The polarizabilities $\alpha_\parallel$, $\alpha_\perp$, of this hydrocarbon chain when the electric field vector $\boldsymbol{E}$ of the radiation is parallel ($\parallel$) or perpendicular ($\perp$) to the chain axis are such that $\alpha_\parallel > \alpha_\perp$.

In the case of the polyethylene plaque it might be expected that the molecular orientation accompanying mould filling would be similar to that observed in polystyrene, Section 4.1.2. In the model of the spherulite, the polymer chains were normal to the ribbon-like crystals, Fig. 13. Thus if the flow-induced molecular orientation is parallel to the *xy* plaque surface, the ribbon crystals will be arranged parallel to each other in the *z* direction. This would seem to be confirmed by the SEM and optical micrographs, Section 3.3, in which the "fibrous" nature of the moulded polyethylene polymer was seen to persist throughout the thickness of the plaque to within approximately 4 μm of each *xy* plaque surface. The fibres (ribbon crystals), approximately 0.1 μm diameter, are generally aligned in the *z* direction (at E5) and birefringence measurements on the *yz* face, Section 3.4.1, gave $n_y > n_z$ which is consistent with the molecules being aligned in the *y* (flow) direction perpendicular to the fibres.

Refractive index measurements on the xy face of E5, Section 3.4.1, gave $n_y = n_x$ and not $n_y > n_x$. This is almost certainly because the flow-induced molecular (and hence fibre) orientation does not extend to the xy plaque surface. The disordered state of the xy surface molecules is that of the boundary layer set down by the fountain flow front., Fig. 12, disturbed by the roughness of the mould surface, Section 3.2.

5. Conclusions

5.1. Polystyrene

The plaque birefringence isochromats had the expected shape of a fluid front entering and filling the mould, the sign and magnitude of the birefringence being determined by the degree of molecular orientation imposed by the flow process. The reduction in birefringence which occurred on annealing the plaque was primarily due to phenyl group reorientation, the molecular disorganization (accompanying stress relaxation and producing distortion) occurring in a number of stages and at a much slower rate. Changing the moulding parameters by increasing T_s, T_m has the effect of thermal annealing by reducing the plaque birefringence, and the magnitude of the "frozen-in" strain; there is also an associated small, but systematic, increase in the mean plaque density, ϱ [1].

5.2 Polyethylene

Microscopic examination of the polyethylene plaques, together with birefringence measurements, showed that the flow-induced molecular orientation persisted throughout the plaque thickness apart from molecularly disordered thin ($\sim 4\,\mu$m) surface layers. Increasing the mould temperature, T_m, increases the mean plaque density, ϱ [1], attributed to associated changes in percentage crystallinity, but produces no visible change in the structural morphology. There is, however, an associated increase in the microhardness, [1] of the molecularly disordered layer forming the plaque surface.

Acknowledgements

The author gratefully acknowledges the advice and cooperation of J. Roberts and R. A. Tickner of RARDE. The work described here was done under contract with the Procurement Executive of the UK Ministry of Defence.

References

1. B. L. EVANS, *J. Mater. Sci.* **24** (1989) 173.
2. B. T. A. CHANG and J. C. M. LI, *ibid.* **15** (1980) 1364.
3. M. R. KANTZ, H. D. NEWMAN and F. H. STIGALE, *J. Appl. Polym. Sci.* **16** (1972) 1249.
4. V. TAN and M. R. KAMAL, *J. Appl. Polym. Sci.* **22** (1978) 2341.
5. M. FUJIYAMA, H. AWAYA and S. KIMURA, *ibid.* **21** (1977) 3291.
6. M. M. QAYYUM and J. R. WHITE, *Polymer* **23** (1982) 129.
7. J. F. RUDD and E. F. GURNEE, *J. Appl. Phys.* **28** (1957) 1096.
8. F. H. MULLER, *Kolloid-Z* **95** (1941) 138.
9. *Idem, ibid.* **95** (1941) 306.
10. J. BAILEY, *India Rubber World* **118** (1948) 225.
11. H. KOLSKY, *Nature* **116** (1950) 235.
12. R. HILTSCHER, *VDI-Z.* **95** (1953) 777.
13. E. F. GURNEE, L. T. PATTERSON and R. D. ANDREWS, *J. Appl. Phys.* **26** (1956) 1106.
14. K. KAWATA, *J. Polymer Sci.* **19** (1956) 359.
15. J. DVORAK and J. MAJER, *Collection. Czechoslov, Chem. Commun.* **22** (1957) 379.
16. H. KOLSKY and A. C. SHEARMAN, *Proc. Phys. Soc. (London)* **55** (1943) 383.
17. L. E. NIELSEN and R. BUCHDAHL, *J. Chem. Phys.* **17** (1949) 839.
18. R. D. ANDREWS and J. F. RUDD, *J. Appl. Phys.* **27** (1956) 990.
19. R. SIGNER, *Trans. Farad. Soc.* **32** (1936) 296.
20. R. D. ANDREWS and T. J. HAMMACK, *J. Polym. Sci. C* **5** (1964) 101.
21. R. D. ANDREWS and J. F. RUDD, *J. Appl. Phys.* **28** (1957) 1091.
22. J. L. S. WALES, "The application of flow birefringence to rheological studies of polymer melts" (Delft University Press, 1976).
23. K. ODA, J. L. WHITE and E. S. CLARK, *Polym. Engng Sci.* **18** (1978) 53.
24. R. L. BALLMAN, T. SHUSHMAN and H. L. TOOR, *Mod. Plast.* **37** (1959) 105.
25. I. M. BARRIE, *Plast. Polym.* **37** (1969) 463.
26. M. R. KAMAL and S. KENIG, *Polym. Engng Sci.* **12** (1972) 294.
27. J. L. BERGER and C. G. GOGOS, *ibid.* **13** (1973) 209.
28. J. L. WHITE, *ibid.* **15** (1975) 44.
29. M. R. KAMAL, Y. KUO and P. H. DOAN, *ibid.* **15** (1975) 863.
30. E. BROYES, C. GUTFINGER and Z. TADMOR, *Trans. Soc. Rheol.* **19** (1975) 423.
31. J. F. STEVEN, A. GALSKY, K. K. WANG, I. CHEN, and D. H. REBER, *Polym. Engn. Sci.* **17** (1977) 666.
32. J. L. WHITE and W. DIETZ, *ibid.* **19** (1979) 1081.
33. A. I. ISAYEV and C. A. HIEBER, *Rheol. Acta.* **19** (1980) 168.
34. M. R. KAMAL and H. HYUN, *ibid.* **12** (1976) 263.
35. L. HOARE and D. HULL, *Polym. Engng Sci.* **17** (1977) 204.
36. R. L. BALLMAN and H. TOOR, *Mod. Plast.* **38** (1960) 113.
37. Z. BAKERDJIAN and M. R. KAMAL, *Polym. Engng Sci.* **17** (1977) 96.
38. M. FLEISSNER, *Kunststoffe* **63** (1973) 597.
39. W. KNAPPE, *ibid.* **51** (1961) 562.
40. A. PELTER, *Plastrerarbeiter* **18** (1967) 883.
41. M. RIGDAHL, *Int. J. Polym. Mater.* **5** (1976) 43.
42. L. D. COXON and J. R. WHITE, *Polym. Engng Sci.* **20** (1980) 230.
43. D. C. BASSETT, "Principles of Polymer Morphology" (Cambridge University Press, Cambridge, 1981).

Received 15 August
and accepted 7 December 1988